Snail locomotion

Sam Pegler,
advised by Neil Balmforth

1 Introduction

A snail propels itself by deforming a layer of mucus beneath it via muscular contractions in its foot muscle. This unique form of locomotion allows snails to traverse almost any obstacle, including the ability to climb steep inclines. Throughout the snail kingdom, there exist a number of variations for the pattern of muscular forcing used by the foot to activate locomotion and in particular, the two main classes of snails, namely land snails and water snails, have adopted two very different patterns. Water snails prefer a method in which its foot applies a predominantly vertical force upon the mucus layer as a wave travelling in the opposite direction to that of locomotion. This *retrograde* locomotion generates forces in a similar manner to that of a peristaltic pump, whereby the forcing surface undergoes significant perpendicular deformation. Land snails prefer a method that applies a wave of tangential muscular contractions that travel in same direction to that of locomotion. Unlike the retrograde case, this *prograde* locomotion involves significant tangential contraction of the base of the foot muscle, and little vertical deformation. These processes involve a rich mixture between the fluid mechanics of the mucus layer and its interaction with the muscular and elastic mechanics of the snail's foot.

A further complication is introduced by the non-Newtonian rheology of snail mucus, which is known to have an appreciable yield stress, i.e, a minimum stress necessary to deform it. Evolution has lead to this rheology because it allows the snail to remain adhered to a steep incline without having to apply any force to counteract its weight. By selectively forcing the mucus in a wave-like pattern, the snail is able to climb the incline without slipping. In this report we investigate the two forms of snail locomotion outlined above, and further attempt to quantify the role of yield stress in locomotion.

Studies of locomotion in fluids began with the seminal work of Taylor [4], who considered the low-Reynolds number problem of a two-dimensional surface surrounded by a Newtonian fluid, that swims by exerting a normal force as a wave travelling in the opposite direction to that of locomotion. By performing a biharmonic analysis of the flow in the limit of a low-amplitude forcing, he relates the velocity of locomotion to the parameters of the forcing. This problem was generalized by Katz [3] to include a rigid wall lying parallel to the swimmer, which he investigates using both the biharmonic approach of Taylor, and a lubrication theory for the thin-gap limit. More recently, Balmforth, Coombs and Pachman [1] extend this lubrication theory to cases involving non-Newtonian fluids in the thin-gap geometry. This study, which considers the effect of a yield stress, is of relevance to the process of retrograde snail locomotion. A model of prograde snail locomotion is investigated
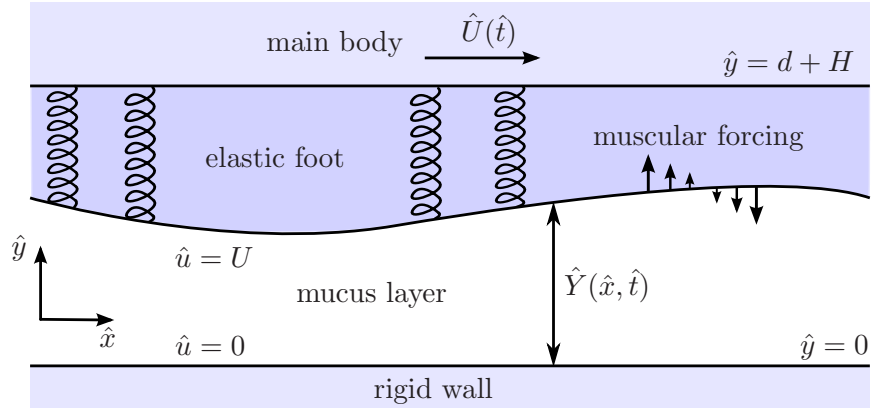
Figure 1: Schematic of the foot and mucus layer in retrograde locomotion.

by Chan, Balmforth and Hosoi [2], in which they model the foot by prescribing its tangential displacement.

In this project, we begin in section 2 with an investigation into the process of retrograde snail locomotion that extends the work of Balmforth *et al.* [1] by solving the system as an initial-value problem, and further explores the effect of the elastic parameters of the foot on the locomotion velocity. We show that the system converges toward a steady state, which we proceed to study by solving the associated eigenvalue problem. From our solutions, we identify a critical yield stress above which locomotion does not occur, and further relate the locomotion velocity to the parameters of the system. In section 3, we consider the case of prograde snail locomotion in which we extend the work of Chan *et al.* [2] by developing a fully dynamic model with both a muscular forcing and a consideration of the elastic mechanics of the snail's foot. We proceed to study the resulting system numerically and derive some analytical results.

2 Retrograde locomotion

2.1 The foot

We assume a configuration in which a layer of mucus of average height H, is confined between the foot's surface at $\hat{y} = \hat{Y}(\hat{x}, \hat{t})$, and a stationary rigid wall at $\hat{y} = 0$, as depicted schematically in figure 1. The foot is assumed to be composed of a linear elastic material, of average thickness d, that lies in contact with the main body of the snail at $\hat{y} = H + d$, which we assume to be a rigid solid that is able to translate horizontally with velocity $\hat{U}(\hat{t})$. Further, we allow the foot to subject itself to forces via internal muscular contractions, which lead to elastic deformation and hence provide a means to activate its motion. Analysis of snail anatomy has shown that these contractions are produced by a series of muscular fibres inclined at varying angles that lie anchored just inside the main body of the snail and the base of the foot. By choosing the contraction pattern of these inclined fibres appropriately, the snail is able to force different points of its foot's surface in a variety of directions and patterns.

In retrograde locomotion, the contraction pattern is such that the resultant muscular forces act predominantly normal to the interface between the mucus layer and the foot, as shown in figure 1. Anatomical studies of snails have shown that the top surface of the foot does not deform significantly into the main body of the snail. Thus, we assume that the main body of the snail acts as a rigid foundation, such that the top surface of the foot does not penetrate the main body above. Assuming the foot is very slender $d \ll L$, where L is a characteristic length scale for its horizontal variation, the leading-order pressure in the foot is given by

$$\hat{p} = \hat{A}f(\hat{x}, \hat{t}) + \hat{D}_R(\hat{Y} - H), \tag{1}$$

where $\hat{A}f$ represents the muscular forcing, $\hat{A}$ is the amplitude of the forcing, and $\hat{D}_R$ is the vertical stiffness coefficient that can be expressed in terms of the elastic parameters of the foot. The elastic force, represented by the second term on the right-hand side of this equation, provides a restoring force that is proportional to the perturbation of the thickness profile from H. Thus, we can consider the surface of the foot to be equivalent to a sheet attached to the main body of the snail via Hookean springs of equilibrium height d, as illustrated in figure 1, where $\hat{D}_R$ represents the Young's modulus of the springs. Based on observations of wave-like patterns of muscular contraction that propagate along the feet of water snails, we assume a forcing of the form

$$f = f(k\hat{\xi}), \tag{2}$$

where $\hat{\xi} = \hat{x} + c\hat{t}$. For positive wave speed c, equation (2) corresponds to a wave travelling in the negative $\hat{x}$-direction, chosen in anticipation that this will lead to steady locomotion in the positive $\hat{x}$-direction.

The absence of significant tangential forcing implies that we can assume that the foot undergoes negligible horizontal deformation to leading order. In this case, the horizontal velocity of the entire foot is equal to that of the main body of the snail $\hat{U}$, so that the velocity of the foot's surface is given uniformly by

$$\hat{u}_s = \hat{U}(\hat{t}). \tag{3}$$

Having established the fundamentals of the foot mechanics in retrograde locomotion, we proceed to consider the fluid mechanics of the mucus layer, which we subsequently relate to the elastic mechanics of the foot via boundary conditions imposed at the foot–mucus interface.

2.2 The mucus layer

We assume that the mucus layer is composed of an incompressible yield-stress fluid that is subject to forcing from the foot above. We proceed to detail a model for the yield-stress rheology of the fluid, and then simplify the theoretical analysis of the resulting equations by applying a lubrication approximation. The general equations of force balance and continuity
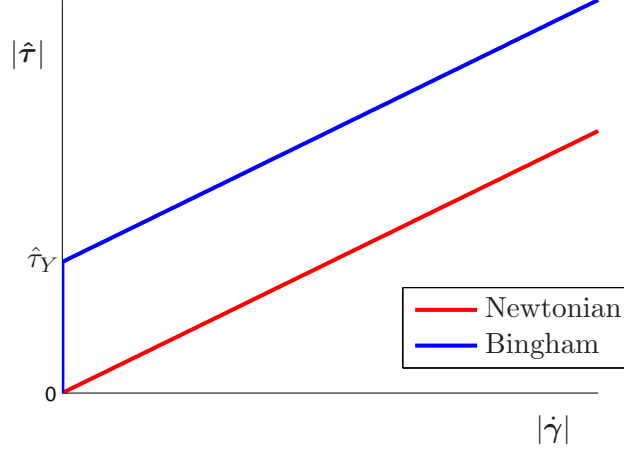
Figure 2: Relationship between the moduli of the deviatoric stress and rate-of-strain tensors for a Newtonian (a) and Bingham (b) fluid.

for an incompressible fluid of velocity $\hat{\boldsymbol{u}} = (\hat{u}, \hat{v})$, are given by

$$\boldsymbol{\nabla} \cdot \hat{\boldsymbol{\tau}} = \boldsymbol{\nabla}\hat{p}, \tag{4}$$

$$\boldsymbol{\nabla} \cdot \hat{\boldsymbol{u}} = 0, \tag{5}$$

where $\hat{\boldsymbol{\tau}}$ is the deviatoric stress tensor, and $\hat{p}$ is the pressure. A constitutive relation that relates the deviatoric stress to the deformation of the fluid is necessary to close the system. The simplest model of a yield-stress fluid is the Bingham model, in which one applies the constitutive relation

$$\begin{cases} \hat{\boldsymbol{\tau}} = \mu\dot{\boldsymbol{\gamma}} + \hat{\tau}_Y \dot{\boldsymbol{\gamma}}/|\dot{\boldsymbol{\gamma}}| & (|\hat{\boldsymbol{\tau}}| > \tau_Y), \\ \dot{\boldsymbol{\gamma}} = \mathbf{0} & (|\hat{\boldsymbol{\tau}}| < \tau_Y), \end{cases} \tag{6a, b}$$

where $\dot{\boldsymbol{\gamma}} \equiv \boldsymbol{\nabla}\hat{\boldsymbol{u}} + (\boldsymbol{\nabla}\hat{\boldsymbol{u}})^T$ is the rate-of-strain tensor, $|\dot{\boldsymbol{\gamma}}| \equiv \sqrt{\dot{\boldsymbol{\gamma}} : \dot{\boldsymbol{\gamma}}}$ and $|\hat{\boldsymbol{\tau}}| \equiv \sqrt{\hat{\boldsymbol{\tau}} : \hat{\boldsymbol{\tau}}}$ are the moduli of the rate-of-strain and deviatoric stress tensors respectively, the constant τ_Y is the yield stress, and μ is the coefficient of viscosity. Relation (6b) ensures that the fluid does not deform if the magnitude of the deviatoric stress at a point does not exceed the yield stress. If the magnitude of the deviatoric stress does exceed the yield stress, then relation (6a) implies that the magnitude of the deviatoric stress in excess of the yield stress is linearly proportional to the deformation of the fluid $\dot{\gamma}$. We sketch this relationship in figure 2, in which we compare it to the Newtonian subcase $\tau_Y = 0$.

Part of the integration of the boundary-value problem defined by equations (4)–(6) involves identifying the locations of yield surfaces where the magnitude of the deviatoric stress tensor attains the yield stress. These surfaces provide boundaries for rigid regions of unyielded fluid, called rigid plugs, in which the magnitude of the deviatoric stress tensor does not exceed the yield stress. Apart from along the yield surfaces, the stress inside these rigid plugs does not form part of the solution described by the Bingham model. The presence of the non-linear yield-stress term in equation (6a), and the need to identify yield surfaces, have the potential to make problems involving Bingham fluids especially difficult

to investigate theoretically. However, given that the thickness of the mucus layer is much less than the characteristic length scale L of its horizontal variation, we can simplify the equations of motion substantially by making a lubrication approximation $H \ll L$. Under this assumption, a scaling analysis of the terms in equation (4) implies that the vertical shear stress $\hat{\tau} = \hat{\tau}_{xy}$ is much greater than the other components of the deviatoric stress tensor. Furthermore, the scaling between horizontal and vertical velocity gradients given by the continuity equation (5) implies that the flow is predominantly horizontal. Thus, to leading order in the lubrication approximation, the horizontal and vertical components of equation (4) simplify to

$$\hat{\tau}_{\hat{y}} = \hat{p}_{\hat{x}}, \tag{7}$$

$$\hat{p}_{\hat{y}} = 0, \tag{8}$$

respectively, while the continuity equation (5),

$$\hat{u}_{\hat{x}} + \hat{v}_{\hat{y}} = 0, \tag{9}$$

remains unchanged. Furthermore, the constitutive relation (6) can be simplified to

$$\begin{cases} \hat{\tau} = \mu \hat{u}_{\hat{y}} + \tau_Y \operatorname{sgn}(\hat{u}_{\hat{y}}) & (|\hat{\tau}| > \tau_Y), \\ \hat{u}_{\hat{y}} = 0 & (|\hat{\tau}| < \tau_Y), \end{cases} \tag{10a, b}$$

where the direction of deformation is given simply by the sign of the vertical shear $\operatorname{sgn}(\hat{u}_{\hat{y}})$. The reduced equations (7)–(8) represent a balance between the divergence of vertical shear stress and the horizontal gradient of the pressure, which is independent of the vertical coordinate at each $\hat{x}$-location.

For retrograde snail locomotion, equations (7)–(10) are subject to the following no-slip conditions on the upper and lower surfaces

$$\hat{u} = \hat{U}(\hat{t}) \qquad (\hat{y} = \hat{Y}), \tag{11}$$

$$\hat{u} = 0 \qquad (y = 0), \tag{12}$$

respectively. Furthermore, the equation for the pressure at the foot's surface (1), combined with continuity of normal stress, implies that the fluid pressure is given by

$$\hat{p} = \hat{A}f + \hat{D}_R\hat{Y} \qquad (\hat{y} = \hat{Y}), \tag{13}$$

to leading order in the lubrication approximation, where we have absorbed the constant $\hat{D}_R H$ into the pressure. Equation (8) implies that the pressure given by (13) applies throughout the vertical extent of the layer at each $\hat{x}$-location. In the following analysis, we assume a sinusoidal muscular forcing of the form

$$f = \sin[k(\hat{x} + c\hat{t})] = \sin(k\hat{\xi}). \tag{14}$$

Noting that this forcing can be considered steady with respect to the variable ξ, we proceed to use ξ in favour of the $\hat{x}$-coordinate. Thus, we recast the system in terms of $(\hat{\xi}, \hat{t})$, and

transform partial derivatives according to

$$\frac{\partial}{\partial \hat{x}} \mapsto \frac{\partial}{\partial \hat{\xi}},\tag{15}$$

$$\frac{\partial}{\partial \hat{t}} \mapsto \frac{\partial}{\partial \hat{t}} + c\frac{\partial}{\partial \hat{\xi}}.\tag{16}$$

We proceed to assume that all variables in the system are 2π-periodic in $k\hat{\xi}$.

On the assumption that the only surface force applied on the main body of the swimmer is from the mucus layer, we can derive an equation for the acceleration of the main body of the snail in terms of the tangential force applied by the mucus along the underside of the foot,

$$\hat{M}\frac{d\hat{U}}{d\hat{t}} = \frac{k}{2\pi}\int_0^{2\pi/k} p\hat{Y}_{\hat{\xi}} + \hat{\tau}_s \, d\hat{\xi} = \langle \hat{\tau}_0 \rangle,\tag{17}$$

where $\hat{M}$ represents the mass of the main body of the snail per unit wavelength, $\hat{\tau}_0 \equiv \hat{\tau}(\hat{\xi}, 0, \hat{t})$, $\hat{\tau}_s \equiv \hat{\tau}(\hat{\xi}, \hat{Y}, \hat{t})$, and the angled brackets denote the average $\langle \phi \rangle \equiv \frac{k}{2\pi}\int_0^{2\pi/k} \phi \, d\hat{\xi}$. The second equality in (17) is derived by applying integration by parts to the pressure term, and using equations (7)–(8) to rewrite the resulting integrand in terms of the stress at the lower surface.

We can derive an evolution equation for the thickness profile by depth-integrating the continuity equation (24) over the thickness of the layer, to yield

$$\frac{\partial \hat{Y}}{\partial \hat{t}} + \frac{\partial \hat{q}}{\partial \hat{x}} = 0,\tag{18}$$

or in terms of $(\hat{\xi}, \hat{t})$,

$$\frac{\partial \hat{Y}}{\partial \hat{t}} + \frac{\partial \hat{Y}}{\partial \hat{\xi}} + \frac{\partial \hat{q}}{\partial \hat{\xi}} = 0,\tag{19}$$

where the flux is defined by $\hat{q}(\hat{\xi}, \hat{t}) = \int_0^{\hat{Y}} \hat{u} \, d\hat{y}$.

We non-dimensionalize the system above according to

$$\hat{\xi} = \frac{1}{k}\xi, \qquad \hat{y} = Hy, \qquad \hat{Y} = HY, \qquad \hat{t} = \frac{1}{kc}t,$$

$$\hat{u} = cu, \qquad \hat{U} = cU, \qquad \hat{\tau} = \frac{\mu c}{H}\tau, \qquad \hat{p} = \frac{\mu c}{kH^2}p.\tag{20}$$

where dimensionless variables are denoted without the hat symbol. In terms of dimensionless variables, equations (7)–(8) become

$$\tau_y = p_\xi,\tag{21}$$

$$p = A\sin\xi + DY,\tag{22}$$

respectively, and the constitutive relation (6) becomes

$$\begin{cases} \tau = u_y + B\mathrm{sgn}(u_y) & (|\tau| > B), \\ u_y = 0 & (|\tau| < B). \end{cases} \qquad (23a, b)$$

The equations of average thickness and depth-integrated continuity become

$$\langle Y \rangle = 1, \quad Y_t + Y_\xi + q_\xi = 0, \qquad (24)$$

the boundary conditions (11)–(12) become

$$u = U(t) \qquad (y = Y), \qquad (25)$$
$$u = 0 \qquad (y = 0), \qquad (26)$$

and the equation-of-motion of the body (17) becomes

$$\dot{U} = \frac{1}{M}\langle \tau_0 \rangle, \qquad (27)$$

where

$$A = \frac{kH^2\hat{A}}{\mu c}, \quad D = \frac{kH^3\hat{D}_R}{\mu c}, \quad B = \frac{H\tau_Y}{\mu c}, \quad M = \frac{Hck\hat{M}}{\mu}, \qquad (28)$$

are the non-dimensional amplitude, non-dimensional stiffness, Bingham number, and non-dimensional mass of the main body per unit wave length, respectively. The Bingham number can be considered a non-dimensional yield stress.

The system above defines an initial-value problem for the evolution of the free boundary $Y(\xi,t)$ and the locomotion velocity $U(t)$. To solve it, we can integrate equations (21)–(23) subject to the boundary conditions (26)–(25) for the velocity profile, given $Y(\xi,t)$ and $U(t)$ at each point in time. With the velocity profiles in hand, we evolve the thickness in time using equation (24), and the locomotion velocity using equation (27), in which the surface stress τ_0 is established as part of the integration for the velocity profiles. The main complication in the above procedure is the construction of the velocity field for a given $Y(x,t)$ and $U(t)$, which we proceed to detail in the following section.

2.3 Construction of the flow profiles

To begin, we can integrate equation (21) with respect to y to yield

$$\tau = \tau_0 + p_\xi y, \qquad (29)$$

where τ_0 is an as yet undetermined function of ξ. This expression for the stress applies in any yielded parts of the flow. Combining equation (29) with the component of the constitutive relation (23a) associated with the yielded regions, provides an equation for the velocity profile in the yielded regions,

$$u_y = \tau_0 + p_\xi y - B\mathrm{sgn}(u_y). \qquad (30)$$

Integrating this equation provides

$$u = \tfrac{1}{2}p_\xi y^2 + [\tau_0 - B\mathrm{sgn}(u_y)]y + K, \tag{31}$$

where K is a constant of integration, which shows that the velocity profiles in the yielded regions of the flow are parabolae.

As part of the solution of the velocity profiles, it is also necessary to determine the locations of any yield surfaces where $|\tau| = B$, which provide the boundaries of any unyielded regions of the flow governed by (23b). We can identify two potential yield surfaces $y = \eta_\pm$ by setting $\tau = \pm B$ in equation (29) to give

$$\eta_\pm = \frac{\tau_0}{p_\xi} \pm \frac{B}{|p_\xi|}, \tag{32}$$

where the modulus of the pressure gradient has been used in the second term on the right-hand side to ensure that $\eta_+ > \eta_-$ independently of the sign of the pressure gradient. We refer to $\eta_\pm$ as potential yield surfaces because it is possible for one, or both, of $\eta_\pm$ to lie outside the domain of the fluid. Equation (32) implies that there exists a region $\eta_- < y < \eta_+$ in which the velocity is independent of the vertical coordinate. Within these regions, the flow is dominated by the yield stress to leading-order in lubrication theory and thus exhibits plug-like characteristics in the vertical direction. We remark that these regions are not true rigid plugs unless their velocity is also independent of the ξ-coordinate. Thus, we refer to regions bounded by the yield surfaces as pseudo-plugs if they are not strictly rigid.

By adding and subtracting the expressions for the potential yield surfaces (32) we deduce that

$$\eta_+ + \eta_- = \frac{2\tau_0}{p_\xi}, \qquad \eta_+ - \eta_- = \frac{2B}{|p_\xi|}, \tag{33a, b}$$

respectively. The latter of these equations provides the width of the pseudo-plug if it lies fully inside the domain, or a maximum for its width if it intersects one of the side walls. The former can be used to relate the positions of the potential yield surfaces to the unknown τ_0.

As mentioned above, it is not necessarily the case that the potential yield surfaces given by equation (32) lie inside the domain of the fluid $0 < y < Y$. For example, if $\eta_+ > 0$ and $0 < \eta_- < Y$, then there exists a pseudo-plug in the region $\eta_- < y < Y$ that intersects the upper surface. In this case the velocity of the pseudo-plug is equal to the velocity of the side wall it is in contact with and the construction of the velocity profile is different to, for example, the regime in which the pseudo-plug lies fully inside the domain. Thus, the different arrangements arising from whether or not one or both of the potential yield surfaces lie inside the domain require consideration on a case-by-case basis. We summarize the equations for the five possible arrangements in appendix A. For the purposes of demonstration, we proceed to construct the velocity profile for regime C, in which the potential locations of the yield surfaces lie inside the boundary of the domain $0 < \eta_\pm < Y$.

We note, by substituting $\tau = \pm B$ into the constitutive relation (23a), that

$$u_y = 0 \qquad (y = \eta_\pm), \tag{34}$$

on the boundaries of the pseudo-plugs, i.e. the vertical gradient of the velocity is continuous at the potential yield surfaces. Combining this condition with the equation for the parabolic profiles in the yielded regions given by (31), we can write down a profile of the form

$$
u = \begin{cases}
u_p + \frac{1}{2}p_\xi(y - \eta_+)^2 & (\eta_+ < y < Y), \\
u_p & (\eta_- < y < \eta_+), \\
u_p + \frac{1}{2}p_\xi(y - \eta_-)^2 & (0 < y < \eta_-),
\end{cases}
\tag{35}
$$

where the plug velocity $u_p = -\frac{1}{2}p_\xi\eta_-^2$ is established on applying condition (26). We determine the remaining unknown in the profile by applying the no-slip condition at the upper interface (25) to give

$$
U = \tfrac{1}{2}p_\xi[(Y - \eta_+)^2 - \eta_-^2].
\tag{36}
$$

Using equation (33b) to eliminate η_- in this equation, and rearranging for the location of the upper yield surface, provides

$$
\eta_+ = \frac{p_\xi^2 Y^2 - 2Up_\xi - 4B^2}{2|p_\xi|(Y|p_\xi| - 2B)}.
\tag{37}
$$

The lower yield surface is then given by

$$
\eta_- = \eta_+ - \frac{2B}{|p_\xi|},
\tag{38}
$$

using equation (33b). Having established the velocity profile (35), we can now derive the flux

$$
q = \tfrac{1}{6}p_\xi[(Y - \eta_+)^3 + \eta_-^3 - 3\eta_-^2 Y],
\tag{39}
$$

which can be used in equation (18) to find the rate-of-change of the thickness profile at each ξ-location. For the evolution of the locomotion velocity, we calculate the integral on the right-hand side of equation (27) using the expression

$$
\tau_0 = \tfrac{1}{2}p_\xi(\eta_+ + \eta_-),
\tag{40}
$$

which is given by rearranging equation (33a).

As shown in appendix A, different regimes have different expressions for the potential yield surfaces. Thus, in constructing the flow profile we determine the regime at a particular ξ-location by calculating the potential yield surfaces in all regimes and then choose the one that is consistent with the regime definition. Note that although the potential yield surfaces for regimes A and E are not used in the expressions for the velocity profiles or fluxes, they are still relevant in the equation for τ_0 given by (40), which we use to evaluate the right-hand side of equation (27).

2.4 Initial-value problem

We solve the initial-value problem described by equations (21)–(27) numerically by applying the Matlab time-integrator `ode15s`, and using fast Fourier transforms to evaluate spatial derivatives. At each step of the time integration, we evaluate the pressure field using
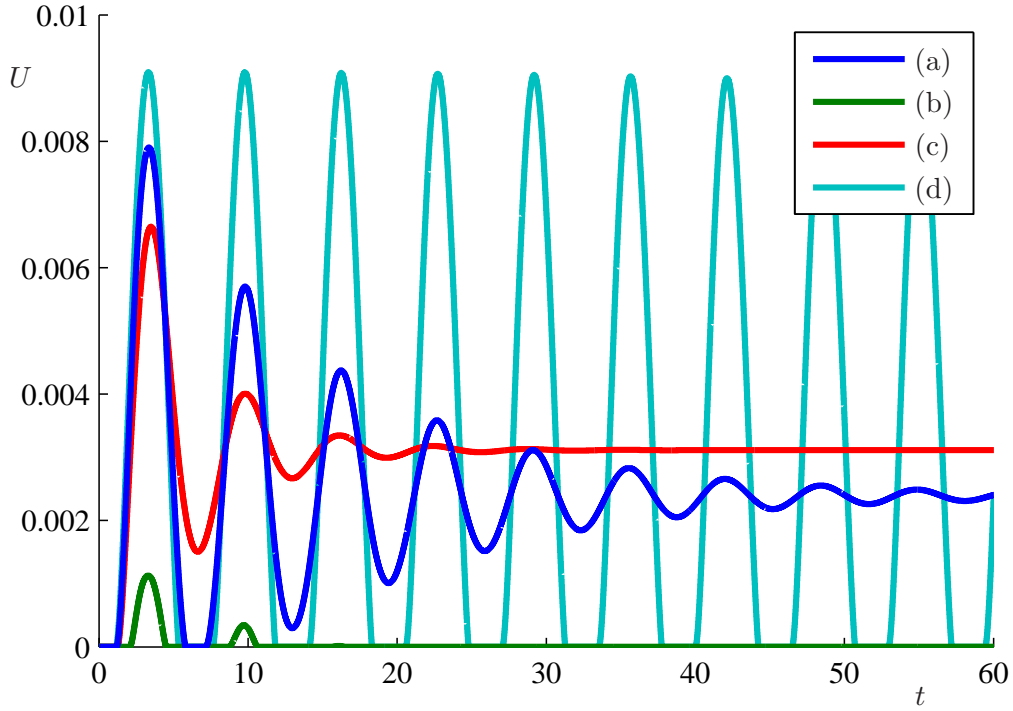
Figure 3: Locomotion velocity as a function of time in the cases (a) $A = 1$, $B = 0.1$, $D = 1$, $M = 1$, (b) $A = 1$, $B = 0.14$, $D = 1$, $M = 1$, (c) $A = 1$, $B = 0.1$, $D = 3$, $M = 1$, and (d) $A = 1$, $B = 0.1$, $D = 0$, $M = 1$.

equation (22), construct the flow profiles using the formulae in appendix A, and use the resulting flux to determine the rate-of-change of the thickness profile using equation (18). Further, we use the formulae for $\eta_\pm$ given in appendix A to evaluate the surface stress τ_0 using equation (40), which we then use to determine the rate-of-change of the locomotion velocity using equation (27). Our solutions for the evolution of the locomotion velocity in the four cases (a)–(d) defined by

(a)	$A = 1$,	$B = 0.1$,	$D = 1$,	$M = 1$
(b)	$A = 1$,	$B = 0.14$,	$D = 1$,	$M = 1$
(c)	$A = 1$,	$B = 0.1$,	$D = 3$,	$M = 1$
(d)	$A = 1$,	$B = 0.1$,	$D = 0$,	$M = 1$

in which we apply the initial conditions

$$\left.\begin{array}{ll} Y & = 1 \\ U & = 0 \end{array}\right\} \ (t = 0), \tag{41}$$

are shown in figure 3. The corresponding evolutions of the thickness profiles in cases (a) and (b) are shown in the space-time plots of figure 4.
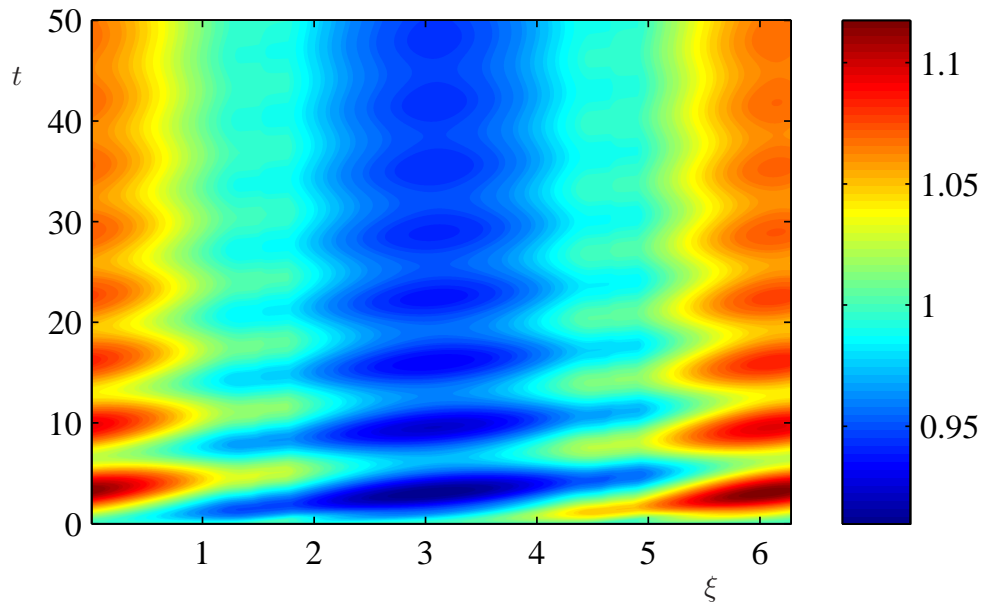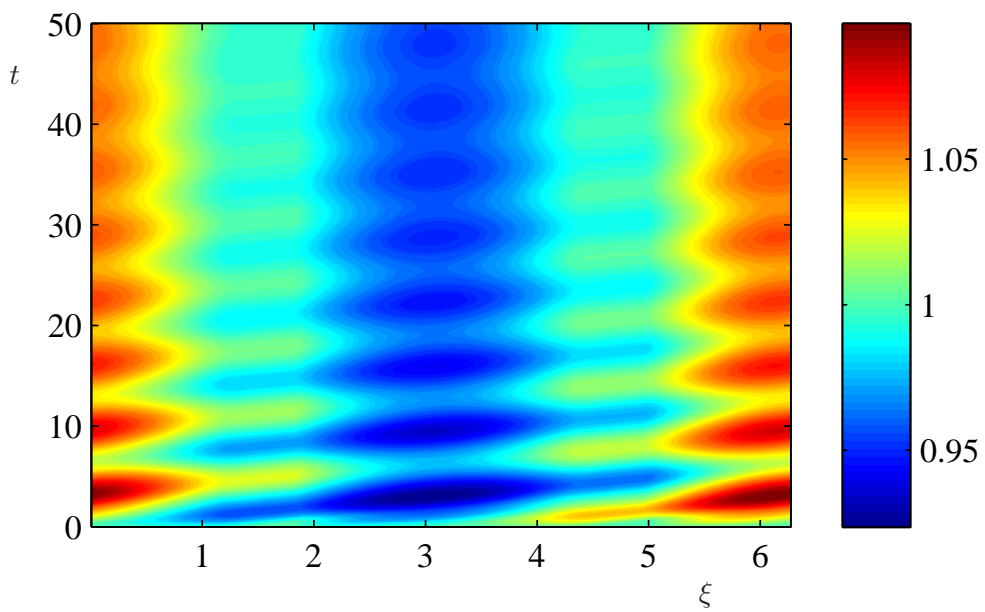
Figure 4: Space-time plots of the evolution of the thickness profile $Y(\xi, t)$ for cases (a) $A = 1$, $B = 0.1$, $D = 1$, $M = 1$, and (b) $A = 1$, $B = 0.14$, $D = 1$, $M = 1$.

For case (a), we observe an initial transient during which the locomotor remains stationary for a short period after its muscles are activated. Although the locomotor is stationary during this initial phase, its thickness profile is strongly time-dependent, as indicated by the space-time plot in figure 4(a). At $t \approx 1.2$, the locomotor rapidly accelerates to a maximum velocity in the first half of the forcing period, and subsequently decelerates back to $U = 0$. After completing a secondary phase of no locomotion, the locomotor subsequently remains in forward motion with a velocity that converges toward a steady value. The oscillation of the locomotion velocity is due to a periodic change in the direction of the tangential stress on the locomotor due to the muscular force wave as it propagates along the foot. By comparing solutions (a) and (c), we observe that a larger stiffness has the effect of reducing the amplitude of the oscillation. In case (d), in which the foot is perfectly inelastic, the locomotor does converge quickly toward a steady state, and appears to remain in a neutrally stable oscillation for all time.

In the limit of large stiffness and large amplitude, the dominant balance in the pressure equation (22) is between the muscular forcing and the stress due to elastic deformation, which recovers the case of imposing the displacement of the foot surface. In this case it is clear that increasing the stiffness has the same effect as reducing the amplitude. Thus, one could hypothesize that increasing the stiffness always reduces the steady-state locomotion velocity. However, we observe that the steady-state velocity of case (c) is greater than that of case (a). This suggests that it is possible to improve locomotion by using a stiffer material where the resultant force due to the muscular forcing and elastic stress is more efficient at creating the tangential stresses on the lower surface of the foot that leads to locomotion.

The observed regions of no locomotion can be explained on the basis that after its inertia vanishes, the locomotor must wait until the muscular and elastic forces can break the yield stress at each ξ-locomotion in order to restart. In case (b), which has a greater Bingham number than case (a), we observe that the locomotor goes through a similar initial transient to that of case (a) but fails to restart on the second oscillation, subsequently converging to a steady state with no locomotion. Thus, we can identify a critical Bingham number $B^*(A, D)$ that lies between the Bingham numbers of cases (a) and (b), which defines the value above which no locomotion occurs in the steady state. We observe from the space-time plot of figure 4(b) that after the locomotor becomes stationary, its thickness profile continues to evolve in time and converges toward a steady-state in a similar manner to that of case (a). Curiously, the locomotor in case (b) has been able to translate forwards despite it coming to a standstill in the steady state, which suggests that it could still be able to locomote by reducing its amplitude over time and then suddenly restarting it at periodic intervals. We proceed to focus our attention on the eventual steady states of the system, in which we identify the value of the critical value B^*.
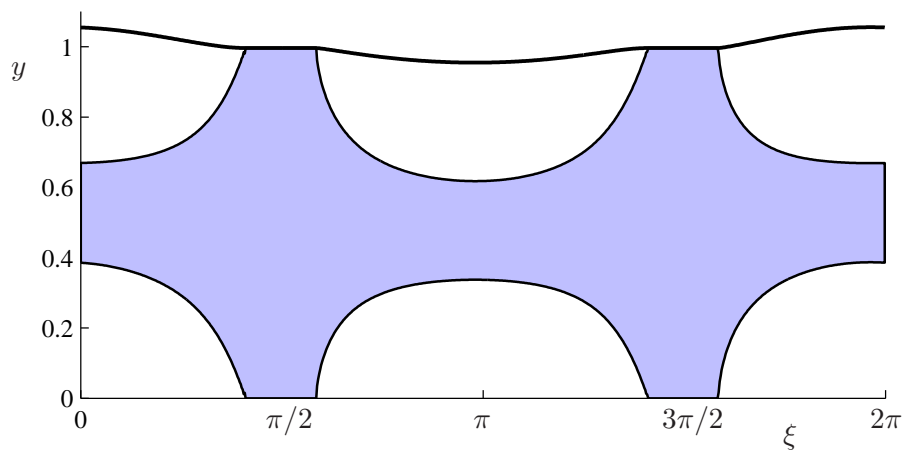
2.5   Steady state

The steady states of the system can be established directly by considering the equations in the case where the time-derivatives are set to zero. In this case, the thickness evolution equation (19) becomes

$$\frac{\partial}{\partial \xi}(Y + q) = 0, \tag{42}$$
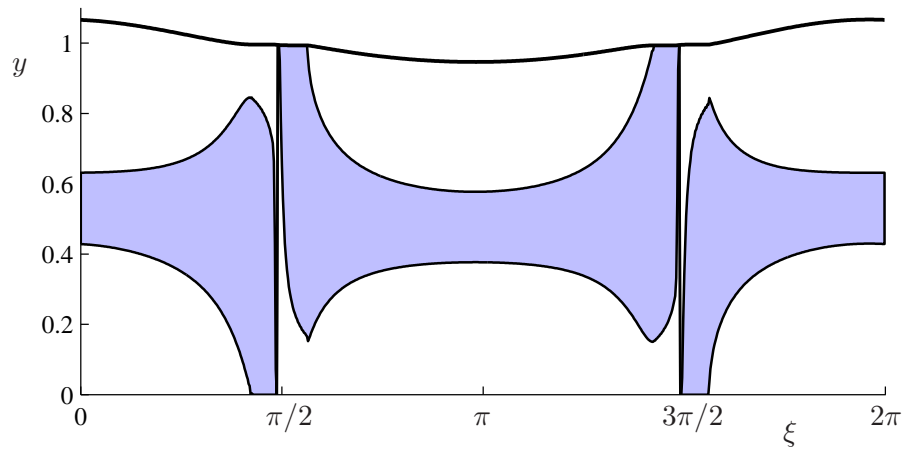
Figure 5: Steady-state profiles in cases (a) $A = 1$, $B = 0.1$, $D = 1$, and (b) $A = 1$, $B = 0.14$, $D = 1$. Regions of unyielded fluid are shown in blue.
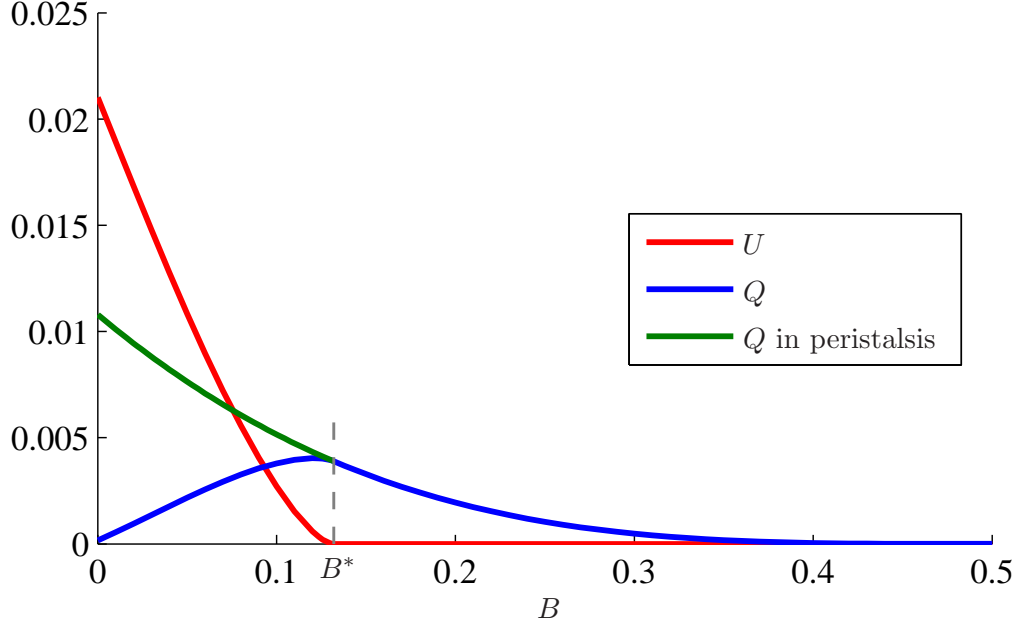
Figure 6: Steady-state locomotion velocity (red), flux (blue), and flux with a fixed locomotor (green), which is relevant to the process of peristalsis, for different values of the Bingham number, in the case $A = 1$, $D = 1$.

which integrates to give

$$Y + q = 1 - Q, \tag{43}$$

where Q is the steady-state flux in the negative ξ-direction. This equation defines an eigenvalue problem for the unknown steady-state thickness profile Y, and the two eigenvalues Q and U, for which we apply the two constraints

$$\langle Y \rangle = 1, \tag{44}$$

$$\langle \tau_0 \rangle = 0, \tag{45}$$

given by the mean thickness condition (24) and the steady form of (27), respectively. We solve this eigenvalue problem numerically using a Newton-Raphson iteration scheme. Noting that trial profiles converge rapidly to the Newtonian case $B = 0$, we initialize the scheme with the Newtonian case and progressively increment B in sufficiently small steps to allow convergence at each step.

Our solutions for the steady-states in cases (a) and (b) are shown in figure 5, and the relationships between the locomotion velocity, flux and Bingham Number in the case $A = 1$, $D = 1$, are shown in figure 6. In case (b), which lies in $B > B^*$, there is no locomotion in the steady state. We see from 5(b) that the thickness profile becomes raised and depressed near the points $\xi = 0$ and $\xi = \pi$, respectively, which correspond to regions where the pressure gradient attains its maximum and minimum values. Furthermore, the yield surfaces touch both the upper and lower boundaries close $\xi = \pi/2$ and $\xi = 3\pi/2$, which are regions where

the pressure gradient becomes close to zero and subsequently changes sign. The plugs in these regions span the vertical extent of the layer, which explains why the locomotor must remain stationary. Although there is no locomotion, there is still fluid motion in the yielded parts of the C-regions, which leads to a net pumping of fluid in the negative ξ-direction. Note that although $q = 0$ in the rigid plugs, it is the steady flux in the wave frame $q + Y$ that is uniform in the above solutions, so it clear that a net transport of fluid is possible with fluid crossing the yield surfaces. In cases such as this in which the locomotor does not move, we can think of the system as being equivalent to that of a peristaltic pump, in which a condition of no horizontal translation on the upper surface would be imposed at all times.

We observe from figure 6 that the flux eventually vanishes at another critical value of the Bingham number. This can be verified by noting that fluid motion stops when the yield surfaces of the C-regions touch the boundaries of the domain everywhere, which first occurs when $\eta_+(\pi) = 1$. Thus, by setting $U = 0$ in equation (88) of appendix A, we deduce that

$$\tfrac{1}{2}Y + \frac{B}{|p_\xi|} = 1, \tag{46}$$

at $\xi = \pi$, on simplification. Further, noting that Y is uniformly equal to one in the fully unyielded steady-state system, equation (22) implies that the pressure gradient at this point is given by $p_\xi(\pi) = -A$. Substituting this value into equation (46) provides the critical value

$$B = \tfrac{1}{2}A. \tag{47}$$

The steady state profile for case (a), displayed in figure 5(a), shows that the pseudo-plugs near $\xi = \pi/2$ and $\xi = 3\pi/2$ do not fully span the vertical extent of the layer. Thus, the locomotor is able to break the yield stress at each ξ-location, leading to a positive locomotion velocity. Figure 6 shows that the locomotion velocity increases as the Bingham number is reduced from B^*, with slow growth in the vicinity of B^*, and approximately linear growth near the Newtonian case $B = 0$. In figure 6, we also compare the corresponding flux in the steady state to that of the peristaltic case, which shows that as the Bingham number is decreased from B^*, the flux soon starts to decrease, but the flux in the peristaltic case continues to increase.

3   Prograde locomotion

3.1   The foot

The defining difference between retrograde and prograde locomotion is given by whether the resultant forcing applied by the foot muscle is predominantly tangential or normal to the surface of the foot. For prograde locomotion, we assume that the contraction pattern of the inclined muscular fibres in the snail's foot is such as to provide a predominantly tangential resultant force at the base of the foot. In this case equations (1)–(3), which were relevant in the retrograde case, no longer apply. Assuming that the main body of the snail acts as a lubricated rigid foundation that does not allow vertical penetration but does allow tangential slip with a no-stress condition, it can be shown that the elastic deformation of
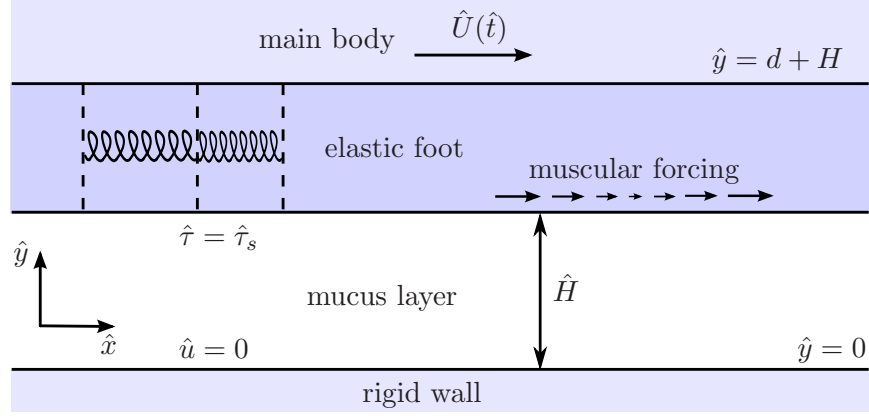
Figure 7: Schematic of the foot and mucus layer in prograde locomotion.

the foot is predominantly horizontal to leading-order in $d \ll L$. Thus, we assume that the base of the foot can undergo significant tangential contraction so that, unlike the retrograde case, we do not impose the condition that the base of the foot moves with the locomotion velocity (3). Instead, we impose a tangential-stress condition,

$$\hat{\tau} = \hat{A}f(\hat{x}, \hat{t}) + \hat{D}_P \hat{u}_{s\hat{x}}, \tag{48}$$

where $\hat{A}f$ is the tangential muscular forcing, $\hat{A}$ is the amplitude of the forcing, and the stiffness coefficient $\hat{D}_P$ can be related to the elastic properties of the foot. The latter term on the right-hand side of this equation represents the elastic force derived from the relative compression of neighbouring points on the foot's surface. Thus, we can think of the foot as a large collection of vertical sections joined by Hookean springs, as illustrated in figure 7. Motivated by observations, we assume a travelling-wave forcing of the form

$$f = f(k\hat{\xi}), \tag{49}$$

where $\hat{\xi} \equiv \hat{x} - c\hat{t}$. For positive wave speed c, this corresponds to a wave that propagates in the positive $\hat{x}$-direction, chosen in anticipation that this will lead to locomotion in the positive $\hat{x}$-direction.

The absence of significant vertical deformation implies that we can assume that the surface of the foot remains in its vertical equilibrium position

$$\hat{Y} = H, \tag{50}$$

at all times. Assuming that the muscular fibres of the foot are anchored inside the main body of the snail, we can define the locomotion velocity of the main body of the snail as the average of the surface velocity,

$$\hat{U} = \langle \hat{u}_s \rangle. \tag{51}$$

The equations above describe the mechanics of a snail's foot undergoing prograde locomotion. We proceed to consider the dynamics of the mucus layer due to the new conditions (48)–(51), and highlight the differences to the retrograde case.

3.2 The mucus layer

In the prograde case, the mechanics of the mucus layer is complicated by the fact that there is no longer a simple expression for the pressure, but is simplified by the fact that it is no longer necessary to evolve the thickness profile in time. The equations of force balance and continuity (7)–(10) are equally relevant in the prograde case, but we no longer assume the surface velocity condition (11) or the pressure condition (13). Instead, equation (48) combined with continuity of tangential stress at the foot's surface, provides a shear-stress condition

$$\hat{\tau} = \hat{\tau}_s = \hat{A}f + \hat{D}_P \hat{u}_{s\hat{\xi}} \qquad (\hat{y} = H). \tag{52}$$

We can non-dimensionalize the relevant equations (7), (8), (10), (12), (19), (50) and (52) according to

$$\hat{\xi} = \frac{1}{k}\xi, \qquad \hat{y} = Hy, \qquad \hat{Y} = HY, \qquad \hat{t} = \frac{1}{kc}t,$$

$$\hat{u} = \frac{H\hat{A}}{\mu}u, \qquad \hat{\tau} = \hat{A}\tau, \qquad \hat{p} = \frac{\hat{A}}{kH}p, \tag{53}$$

where dimensionless variables are denoted without the hat symbol. The resulting non-dimensional equations of force balance are

$$\tau_y = p_\xi, \tag{54}$$
$$p_y = 0, \tag{55}$$

with constitutive relation,

$$\begin{cases} \tau = u_y + R\,\mathrm{sgn}(u_y) & (|\tau| > R), \\ u_y = 0 & (|\tau| < R), \end{cases} \tag{56a, b}$$

and boundary conditions,

$$\tau = \tau_s = f + Du_{s\xi} \qquad (y = 1), \tag{57}$$
$$u = 0 \qquad\qquad\quad (y = 0). \tag{58}$$

The thickness and depth-integrated continuity equations are given by

$$Y = 1, \quad q_\xi = 0, \tag{59}$$

respectively, where in the equations above,

$$R = \frac{\tau_Y}{\hat{A}}, \quad D = \frac{kH\hat{D}_P}{\mu}, \tag{60}$$

are the yield-stress–amplitude ratio, and the non-dimensional stiffness, respectively. The non-dimensionalization above shows that the absence of a scaling between the rate-of-change of the thickness profile and the divergence of flux in the depth-integrated continuity equation (59) implies that unlike the retrograde case, it has been possible to incorporate the yield

stress and amplitude into a single parameter R. We remark that the limit of large stiffness recovers the case of imposing the tangential displacement of the foot's surface.

3.3 Eigenvalue problem

The depth-integrated continuity equation (59) can be integrated to give

$$q = Q, \tag{61}$$

where Q is the flux of fluid in the positive ξ-direction. Thus, the prograde system has been reduced to an eigenvalue problem for the unknown pressure gradient p_ξ and eigenvalue Q, that we solve subject to the periodicity constraint

$$\langle p_\xi \rangle = 0. \tag{62}$$

As in the retrograde case, the main complication is in the construction of the velocity profiles when a yield stress is present. However, before discussing the effects of yield stress, we begin by considering the simpler Newtonian case.

Newtonian solution

In the Newtonian case $R = 0$, we can relate the flux Q and locomotion velocity U to the forcing function analytically. To show this, we begin by integrating equation (70), with the constitutive relation (56) with $R = 0$, to give the parabolic velocity profile

$$u = \tfrac{1}{2} p_\xi y^2 + (\tau_s - p_\xi) y, \tag{63}$$

in which we have applied the condition of no-slip at the base (58). The associated formula for the flux is then given by

$$q = \tfrac{1}{2}\tau_s - \tfrac{1}{3} p_\xi = Q, \tag{64}$$

which is uniformly equal to Q according to (61). Taking the ξ-average of this equation yields

$$Q = \tfrac{1}{2}\langle \tau_s \rangle, \tag{65}$$

on applying the continuity constraint (62). Substituting the expression for the surface stress (57) gives

$$Q = \tfrac{1}{2}\langle f + D u_{s\xi} \rangle = \tfrac{1}{2}\langle f \rangle, \tag{66}$$

noting that the average of the elastic term vanishes. Thus, we have established the flux in terms of the imposed tangential forcing. To determine the associated locomotion velocity, we evaluate the velocity of the fluid at the surface by setting $y = 1$ in equation (63) to give

$$u_s = \tau_s - \tfrac{1}{2} p_\xi. \tag{67}$$

Now, taking the ξ-average of this equation yields

$$U = \langle u_s \rangle = \langle \tau_s \rangle = \langle f + D u_{s\xi} \rangle = \langle f \rangle, \tag{68}$$

on noting again that the average of the elastic term is zero.

Expressions (66) and (68) show that both the flux and the locomotion velocity are linearly related to the mean value of the imposed forcing function f. Thus, we are motivated in our analysis of the non-Newtonian case to prescribe a forcing with a non-zero mean. In this regard, we proceed to impose

$$f = \sin^2 \xi, \tag{69}$$

which has mean value $\langle f \rangle = \frac{1}{2}$. We remark that in adopting this forcing, it is not possible to balance the tangential stress exerted on the main body of the snail without the snail placing the front or back of its foot in contact with the ground to provide a frictional force to balance that of the muscular contractions. The resulting process of locomotion is similar to that of an inchworm, which is known to be adopted occasionally by some land snails.

As a side note, we remark that it is possible to locomote in the case $\langle f \rangle = 0$ if a yield stress is present. To demonstrate this, consider a forcing pattern with small regions of high magnitude forcing in the positive ξ-direction, and with larger regions of low magnitude forcing in the negative ξ-direction, constructed with $\langle f \rangle = 0$, such that only regions of the forcing directed in the direction of locomotion will break the yield stress. Then it is clear that the velocity of the foot surface will be either stationary or directed only in the positive ξ-direction. The mean surface velocity will thus be positive, providing locomotion. Such a pattern may correspond to that adopted commonly by land snails, in cases where the surface of the foot does not make direct contact with the ground.

The effect of yield stress

The effect of yield stress can be established by considering the eigenvalue problem defined by equations (61)–(62), with the forcing (69), in the general case $R \geq 0$. To simplify the analysis, we assume $D = 0$ with the expectation that the resulting system will encapsulate the behaviour of the general case. We solve the eigenvalue problem for the unknown pressure gradient numerically using a Newton-Raphson iteration scheme initialized using the Newtonian solution discussed above. In each iteration, we construct the flow profiles with the pressure gradient form the previous step using an analogous procedure to that outlined in section 2.3. The first step of the integration of the flow profiles can be achieved by integrating (54) subject to (57) to give

$$\tau = f + p_\xi(1 - y), \tag{70}$$

from which we deduce that the potential yield surfaces are given by

$$\eta_\pm = 1 - \frac{f}{p_\xi} \pm \frac{R}{|p_\xi|}, \tag{71}$$

in all regimes. The other formulae associated with the construction of the velocity profiles are summarized in appendix B. For our solution, we plot the dependence of the locomotion velocity and flux on the yield-stress–amplitude ratio R in figure 8, and some examples of yield-surface plots and pressure-gradient profiles for specific values of R are shown in figures 9 and 10, respectively.

In all cases of R, we can define a region of the fluid $|\zeta| < \zeta_D$, where $\zeta \equiv \xi - \pi/2$, and
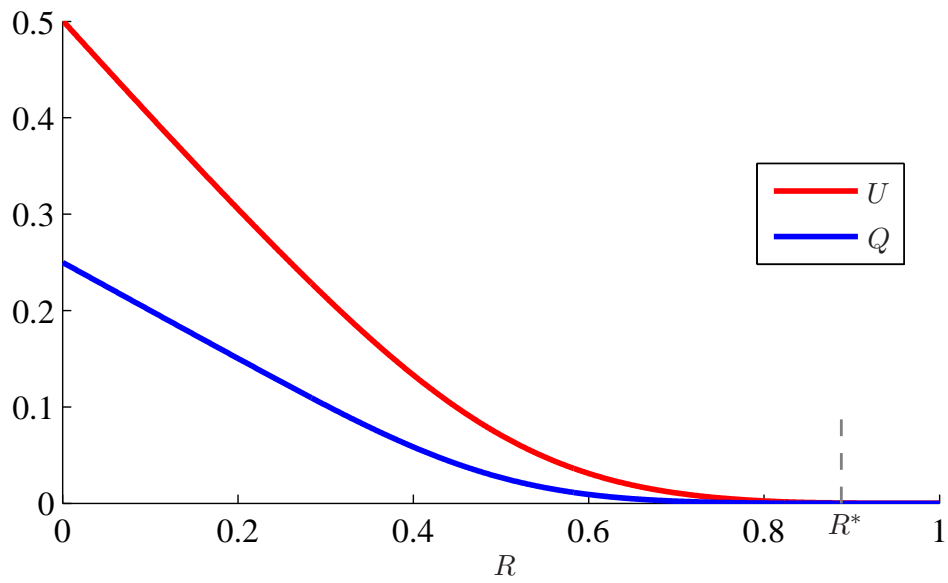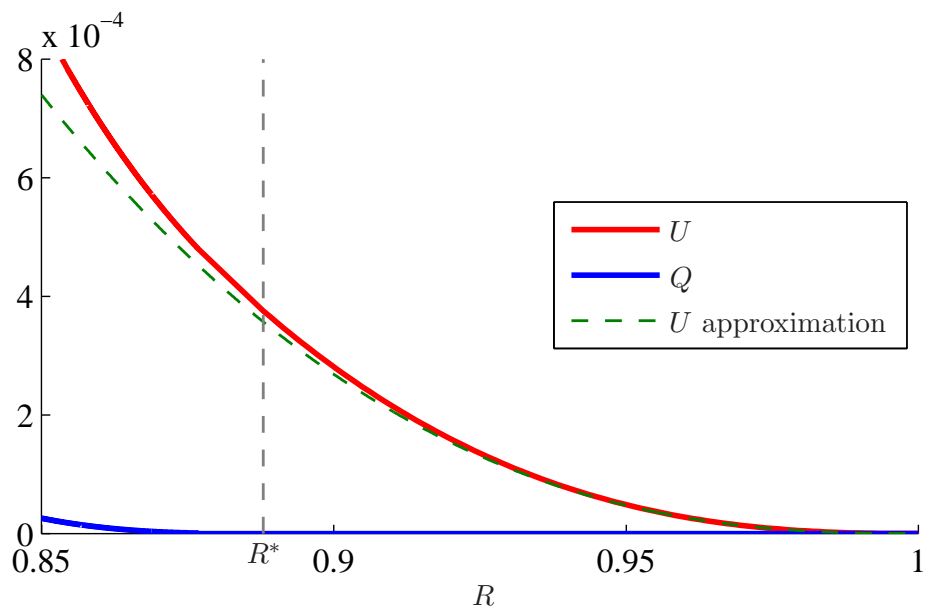
Figure 8: Locomotion velocity and flux in prograde locomotion (a), and a blow-up (b) of the region $R^* < R < 1$, in which we plot the asymptotic approximation (80) for U.

ζ_D is defined by

$$R = \cos^2 \zeta_D, \tag{72}$$

in which the fluid in contact with the foot must be yielded because the imposed tangential forcing at these points exceeds the yield stress. Conversely, the region of the fluid $|\zeta| > \zeta_D$ in contact with the foot $y = 1$ must be unyielded. In order to provide a non-zero flux, it is necessary that the structure of the yield surfaces is such that there is a pseudo-plug extending from the top surface and a flow near the lower surface, corresponding to regime D in appendix B; this is evident in the example profiles of figure 9. Furthermore, we can deduce from equation (70) that the pressure gradient is always negative in the D-region, $|\zeta| > \zeta_D$, and positive elsewhere, which is verified by the pressure-gradient plots of figure 10.

The case $R = 0.2$, shown in figure 9(a), is fully yielded except in the pseudo-plugs of the D-regions discussed above. As R is increased, there is a critical point $R \approx 0.253$, where a pseudo-plug emerges from the base at $\zeta = 0$. This B-region, shown in figure 9(b) for the case $R = 0.6$, proceeds to grow as R is further increased. We observe from figure 8 that the flux remains approximately half the locomotion velocity in the region $0 < R \lesssim 0.4$ and beyond this point, the ratio of the flux to the locomotion velocity begins to decrease at a much faster rate. At $R \approx 0.762$, a C-region appears inside the B-region with a yielded region emerging at the base, and a groove in the upper yield surface, as shown in figure 9(c) for the case $R = 0.8$. At this stage, the regime progression across the period can be summarized

$$D \rightarrow E \rightarrow A \rightarrow B \rightarrow C \rightarrow B \rightarrow A \rightarrow E \rightarrow D, \tag{73}$$

where the letters correspond to the regime definitions given in appendix B. The fully-yielded A- and E-regions, which are too narrow to be discerned clearly in figure 9(c), lie near locations where the pressure gradient changes sign, as can be verified by plot (c) in figure 10. As R is increased further, there is a critical point R^* where the pseudo-plugs in the D-regions touch the base and become rigid plugs that span the thickness of the layer. At this point, the flux vanishes and the velocity of the foot's surface u_s becomes zero within the region $|\zeta| > \zeta_D$. However, the remaining motion of the foot in the C-region $|\zeta| < \zeta_D$ is still able to drive a small locomotion velocity. The behaviour of the flux and locomotion velocity for $R^* < R < 1$ is shown in figure 8(b).

The onset of locomotion

It is clear that there is no fluid motion if $R > 1$ because in this case the shear stress does not exceed the yield stress anywhere in the fluid. As mentioned above, a C-region emerges about $\zeta = 0$ as R is decreased from 1, such that although the fluid flux remains zero, the foot is still able to drive locomotion. This can be contrasted with the retrograde case in which the flux is always non-zero when locomotion occurs. We proceed to solve the eigenvalue problem for the pressure gradient in the case $R^* < R < 1$ by applying the constraint $Q = 0$ in place of the periodicity constraint (62). The latter is abandoned because a solution for the pressure gradient inside the rigid plugs is not determined as part of the Bingham model. We can assume that the periodicity constraint is accounted for via an elastic force balance within the rigid regions that we need not consider explicitly.
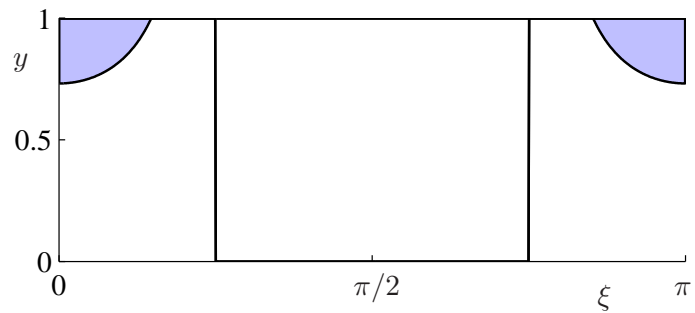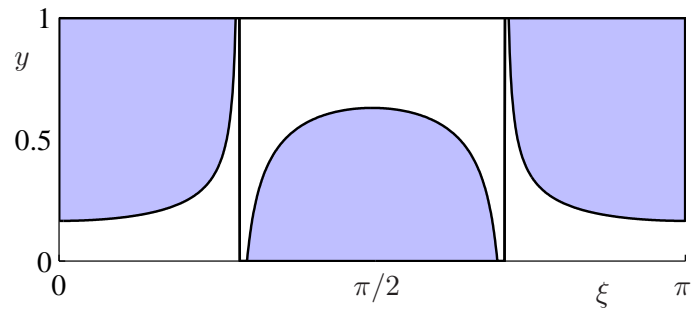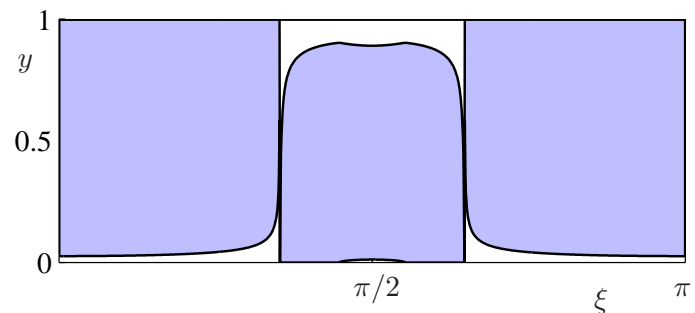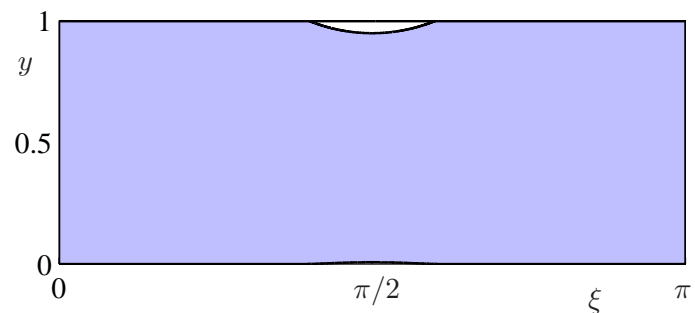
Figure 9: Yield-surface profiles in the cases (a) $R = 0.2$, (b) $R = 0.6$, (c) $R = 0.8$, and (d) $R = 0.9$. Regions of unyielded fluid are shown in blue.
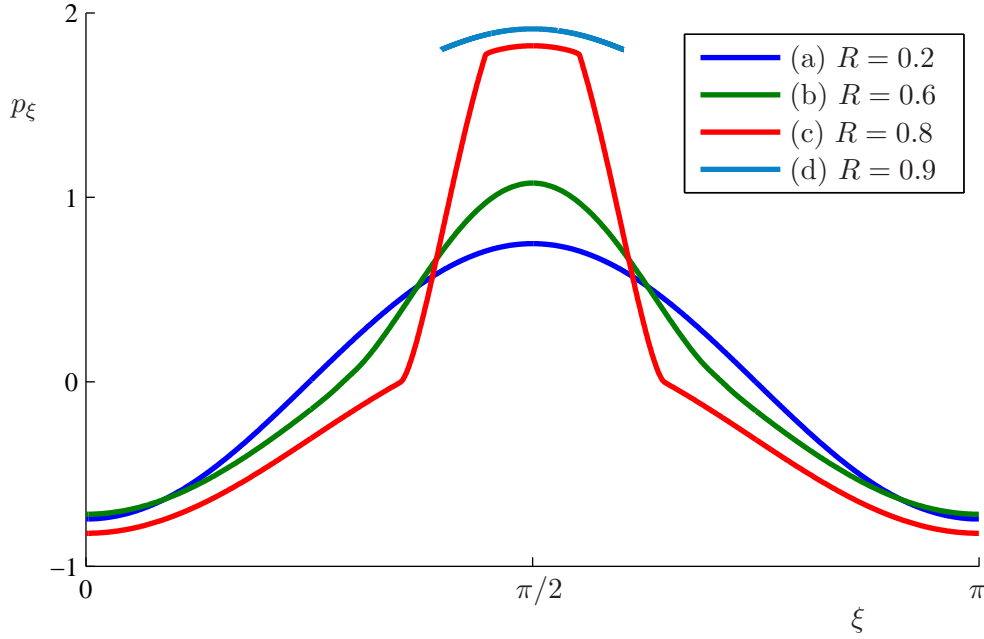
Figure 10: Pressure-gradient profiles in the cases (a) $R = 0.2$, (b) $R = 0.6$, (c) $R = 0.8$, and (d) $R = 0.9$. For case (d), the pressure gradient remains undetermined in the region $|\zeta| > |\zeta_D|$ under the Bingham model.

In the C-region, the condition of zero flux implies that

$$(1 - \eta_+)^3 + \eta_-^2(\eta_- - 3) = 0, \tag{74}$$

using equation (90) from appendix B. Eliminating $\eta_\pm$ in favour of the unknown pressure gradient using equations (71), and recalling that $p_\xi > 0$ for $|\zeta| < \zeta_D$, gives

$$(f - R)^3 - (2p_{C\xi} + f + R)(p_{C\xi} - f - R)^2 = 0, \tag{75}$$

which is an algebraic equation for the pressure gradient $p_{C\xi}$ in the C-region. We solve this cubic equation numerically using the Matlab routine `fzero`. From our solution, we can identify two positive roots if $R < 1$, which in the limit of $R \to 1$, are given by

$$p_{C\xi} \sim f + R \pm \left[\frac{(f - R)^3}{3(f + R)}\right]^{1/2}, \tag{76}$$

to leading order. It can be verified numerically that the lesser root always leads to an inconsistent solution with $\eta_- < 0$. Thus, we use the greater root to calculate the yield surface profiles. Our solution for the yield surface profile in the case $R = 0.9$ is shown in figure 9(d), and the corresponding pressure gradient is shown by plot (d) in figure 10. Furthermore, we use the non-dimensional form of equation (51) to evaluate the locomotion

velocity

$$U = \frac{2}{\pi} \int_0^{\zeta_D} u_s \, \mathrm{d}\zeta, \tag{77}$$

in which the surface velocity is given by

$$u_s = \tfrac{1}{2} p_\xi [(1 - \eta_+)^2 - \eta_-^2] = \frac{(p_\xi - 2R)(2f - p_\xi)}{2p_\xi}, \tag{78}$$

which we have established using equation (89) given in appendix B. We use the resulting solution for U to extend the plot in figure 8(b) to the region $R^* < R < 1$.

In the limit $R \to 1$, an approximation for the surface velocity can be derived by substituting the leading-order form of the pressure gradient given by equation (76) into equation (78) to give

$$u_s \sim \tfrac{1}{4}(1 - R - \zeta^2)^2. \tag{79}$$

Using this expression to evaluate the integral in equation (77) provides

$$U \sim \frac{4}{15\pi}(1 - R)^{5/2}, \tag{80}$$

on noting that $\zeta_D \sim \sqrt{1 - R}$ from equation (72). Figure 8(b) shows that this approximation gives good agreement with the exact solution.

The onset of flux

The critical value R^* defines the point at which the flux first vanishes. Moreover, this point corresponds to the point when both the periodicity constraint (62) and the flux constraint $Q = 0$ are satisfied simultaneously. In reference to the profiles shown in figure 8, we note that as R approaches R^* from below, this critical point is reached when the lower yield surface η_- in the D-region first touches the lower surface such that $\eta_- = 0$. Thus, the pressure gradient in the D-region at the critical point can be found by setting $\eta_- = 0$ in equation (71) to give

$$p_{D\xi} = f - R^*, \tag{81}$$

recalling that $p_\xi < 0$ for $|\zeta| > \zeta_D$. The pressure gradient in the C-region is given by the numerical solution to (75) described above, which along with (81), enters the continuity constraint (62) according to

$$\int_0^{\zeta_D} p_{C\xi} \, \mathrm{d}\zeta + \int_{\zeta_D}^{\pi/2} p_{D\xi} \, \mathrm{d}\zeta = 0, \tag{82}$$

where we have taken the integral over half the period using the fact that the solution is symmetric about $\zeta = 0$. On substituting the pressure gradient in the D-region given by equation (81), and evaluating the second integral, this equation reduces to

$$\int_0^{\zeta_D} p_{C\xi} \, \mathrm{d}\zeta = (R^* - \tfrac{1}{2})(\tfrac{\pi}{2} - \zeta_D) + \tfrac{1}{4}\sin(2\zeta_D). \tag{83}$$

We solve the integro-algebraic system defined by equation (75) with $R = R^*$ and (83) numerically by treating R^* as a shooting parameter. For each trial in this method, we solve the algebraic equation (75) for $p_{C\xi}$ using the Matlab routine `fzero`. Our solution gives the critical value $R^* \approx 0.888$.

A near-exact derivation of this result can be derived semi-analytically with less work by making use of the fact that $R^* \approx 1$, and recalling that in the limit $R \to 1$, equation (76) implies that the pressure gradient in the C-region is given approximately by

$$p_{C\xi} \approx f + R^*. \tag{84}$$

Substituting this expression into equation (83), and simplifying, provides

$$\int_0^{\pi/2} f \, \mathrm{d}\zeta + R^*(2\zeta_D - \tfrac{\pi}{2}) \approx 0, \tag{85}$$

and hence

$$\tfrac{\pi}{4} + R^*(2\zeta_D - \tfrac{\pi}{2}) \approx 0. \tag{86}$$

Using equation (72) to eliminate R^* in this equation leaves the algebraic equation

$$\tfrac{\pi}{4} + (2\zeta_D - \tfrac{\pi}{2})\cos^2 \zeta_D = 0, \tag{87}$$

which can be solved numerically for the solution $\zeta_D \approx 0.343$, with corresponding critical value $R^* \approx 0.887$ calculated using equation (72). Given that this value is very close to the exact value derived previously, we can conclude that the above approximation is successful at describing the region of the parameter space in which R is close to R^*.

4 Conclusion

We have investigated theoretically and numerically models for retrograde and prograde snail locomotion using a dynamic formulation that accounts for both the elastic and muscular mechanics of the snail's foot, and the yield stress of the mucus layer. Our solution of the initial-value problem in the retrograde case shows an initial transient that involves a highly oscillatory locomotion velocity, with the potential for extended periods of no locomotion. We observe a transition toward a steady state in the wave frame of the forcing, which we investigate by finding solutions of the associated steady-state eigenvalue problem. For given values of the non-dimensional forcing amplitude and stiffness, we identify a critical value of the Bingham number above which there is no locomotion in the steady state. In our analysis of prograde locomotion, we find that the locomotor is able to pump fluid in the direction it is travelling only below a critical value of the yield-stress–amplitude ratio, which we have identified in the case of zero stiffness. Beyond this point, the flux vanishes but the snail is still able to locomote.

A notable difference between the two forms of locomotion we have studied is that the flux in the retrograde case is directed in the opposite direction to that of locomotion, while in the prograde case, the snail is able to pump fluid in the direction it is travelling. Given that mucus production is a substantial chemical cost to the snail, this difference may account

351

for why land snails have favoured the prograde form of locomotion. Furthermore, we can hypothesize that a water snail predominantly uses ambient water as a lubricating fluid, and only occasionally produce mucus if, for example, it needs to climb a steep incline.

A   Regimes in retrograde locomotion

Regime A: $(p_\xi U > 0, \; \eta_\pm < 0)$

$$u = \tfrac{1}{2} p_\xi y(y - U) + \frac{Uy}{Y}, \quad q = \tfrac{1}{2} UY - \tfrac{1}{12} p_\xi Y^3,$$

$$\eta_+ = \tfrac{1}{2} Y - \frac{U}{p_\xi Y}, \quad \eta_- = \eta_+ - \frac{2B}{|p_\xi|}.$$

Regime B: $(p_\xi U > 0, \; \eta_- < 0 < \eta_+ < Y)$

$$u = \begin{cases} \tfrac{1}{2} p_\xi (y - \eta_+)^2 & (\eta_+ < y < Y), \\ 0 & (0 < y < \eta_+), \end{cases}$$

where the pseudo-plug is stationary.

$$\eta_+ = Y - \sqrt{\frac{2U}{p_\xi}}, \quad \eta_- = \eta_+ - \frac{2B}{|p_\xi|}.$$

$$q = \tfrac{1}{6} p_\xi (Y - \eta_+)^3.$$

Regime C: $(0 < \eta_\pm < Y)$

$$u = \begin{cases} u_p + \tfrac{1}{2} p_\xi (y - \eta_+)^2 & (\eta_+ < y < Y), \\ u_p & (\eta_- < y < \eta_+), \\ u_p + \tfrac{1}{2} p_\xi (y - \eta_-)^2 & (0 < y < \eta_-), \end{cases}$$

where the plug velocity is given by $u_p = -\tfrac{1}{2} p_\xi \eta_-^2$,

$$\eta_+ = \frac{p_\xi^2 Y^2 - 2U p_\xi - 4B^2}{2|p_\xi|(Y|p_\xi| - 2B)}, \quad \eta_- = \eta_+ - \frac{2B}{|p_\xi|}, \tag{88}$$

$$q = \tfrac{1}{6} p_\xi [(Y - \eta_+)^3 + \eta_-^3 - 3\eta_-^2 Y].$$

Regime D: $(p_\xi U < 0, \; 0 < \eta_- < Y < \eta_+)$

$$u = \begin{cases} u_p & (\eta_- < y < Y), \\ u_p + \tfrac{1}{2} p_\xi (y - \eta_-)^2 & (0 < y < \eta_-), \end{cases}$$

where the plug velocity is given by $u_p = -\frac{1}{2}p_\xi\eta_-^2$.

$$\eta_- = \sqrt{-\frac{2U}{p_\xi}}, \quad \eta_+ = \eta_- + \frac{2B}{|p_\xi|},$$

$$q = \frac{1}{6}p_\xi\eta_-^2(\eta_- - 3Y).$$

Regime E: $(p_\xi U < 0, \eta_\pm > 1)$

$$u = \frac{1}{2}p_\xi y(y - U) + \frac{Uy}{Y}, \quad q = \frac{1}{2}UY - \frac{1}{12}p_\xi Y^3,$$

$$\eta_- = \frac{1}{2}Y - \frac{U}{p_\xi Y}, \quad \eta_+ = \eta_- + \frac{2B}{|p_\xi|}.$$

B   Regimes in prograde locomotion

The potential yield surfaces at $y = \eta_\pm$ are given by

$$\eta_\pm = 1 - \frac{\tau_s}{p_\xi} \pm \frac{R}{|p_\xi|},$$

in all regimes.

Regime A: $(p_\xi > 0, \eta_\pm < 0)$

$$u = \frac{1}{2}p_\xi y^2 + (\tau_s - p_\xi - R)y,$$
$$q = -\frac{1}{3}p_\xi + \frac{1}{2}(\tau_s - R).$$

Regime B: $(p_\xi > 0, \eta_- < 0 < \eta_+ < 1)$

$$u = \begin{cases} \frac{1}{2}p_\xi(y - \eta_+)^2 & (\eta_+ < y < 1), \\ 0 & (0 < y < \eta_+), \end{cases}$$

where the pseudo-plug is stationary.

$$q = \frac{1}{6}p_\xi(1 - \eta_+)^3.$$

Regime C: $(0 < \eta_\pm < 1)$

$$u = \begin{cases} u_p + \frac{1}{2}p_\xi(y - \eta_+)^2 & (\eta_+ < y < 1), \\ u_p & (\eta_- < y < \eta_+), \\ u_p + \frac{1}{2}p_\xi(y - \eta_-)^2 & (0 < y < \eta_-), \end{cases} \tag{89}$$

where the plug velocity is given by $u_p = -\frac{1}{2}p_\xi\eta_-^2$.

$$q = \frac{1}{6}p_\xi[(1 - \eta_+)^3 + \eta_-^3 - 3\eta_-^2]. \tag{90}$$

Regime D: $(p_\xi < 0,\ 0 < \eta_- < 1 < \eta_+)$

$$u = \begin{cases} u_p & (\eta_- < y < 1), \\ u_p + \frac{1}{2}p_\xi(y - \eta_-)^2 & (0 < y < \eta_-), \end{cases}$$

where the plug velocity is given by $u_p = -\frac{1}{2}p_\xi\eta_-^2$.

$$q = \tfrac{1}{6}p_\xi\eta_-^2(\eta_- - 3).$$

Regime E: $(p_\xi < 0,\ \eta_\pm > 1)$

$$u = \tfrac{1}{2}p_\xi y^2 + (\tau_s - p_\xi - R)y,$$
$$q = -\tfrac{1}{3}p_\xi + \tfrac{1}{2}(\tau_s - R).$$

References

[1] N. J. BALMFORTH, D. COOMBS, AND S. PACHMAN, Microelastohydrodynamics of swimming organisms near solid boundaries in complex fluids, Q. J. Mechanics Appl. Math, 63 (2009), pp. 267–294.

[2] B. CHAN, N. J. BALMFORTH, AND A. E. HOSOI, Building a better snail: lubrication and adhesive locomotion, Phys. Fluids, 17 (2005), p. 113101.

[3] D. F. KATZ, Propulsion of microorganisms near solid boundaries, J. Fluid Mech., 64 (1974), pp. 33–49.

[4] G. I. TAYLOR, Analysis of the swimming of microscopic organisms, Proc. R. Soc. A, 209 (1951), pp. 447–461.